From Darkness to Light
ASP Conference Series, Vol. 3×10^8*, 2000*
T. Montmerle & Ph. André, eds.

arXiv:astro-ph/0007298v1 20 Jul 2000

The Low-Mass Stars in Starburst Clusters

Bernhard Brandl, the NGC 3603[1], and the 30 Doradus-Team[2]

Cornell University, 222 Space Sciences Building, Ithaca, NY 14853, USA

Abstract. If star formation depends strongly on the global properties of the environment in which they form, the slope of the IMF as well as the upper and lower mass cut-offs would be expected to vary significantly between violent starbursts and more quiescent star forming regions. To test this hypothesis we observed the stellar content of the two closest massive star forming regions, 30 Doradus and NGC 3603 with HST/NICMOS and VLT/ISAAC. Our observations are the most sensitive observations made to date of dense starburst cores, allowing us to investigate its low-mass stellar population with unprecedented quality. The NIR luminosity function of 30 Doradus shows *no* evidence for a truncation down to at least $1M_\odot$, its stellar core R136 is populated in low-mass stars to at least $2M_\odot$ and NGC 3603, which is very similar to R136, down to $0.1M_\odot$. Our observations clearly show that *low-mass stars do form in massive starbursts.*

1. Introduction

The stellar initial mass function (IMF) [Salpeter (1955), Miller & Scalo (1979), Scalo (1986), Kroupa, Tout & Gilmore (1990), ...] is the distribution of stellar masses at $t = 0$. It is mainly characterized by three parameters: the upper mass cutoff m_u, the lower mass cutoff m_l, and the slope $\Gamma = \frac{d \log \xi(\log m)}{d \log m}$. The values of $\Gamma, m_u,$ and m_l depend on the physical processes that lead to the formation of stars and hence may not be "universal" but depend rather significantly on the environment, i.e., the global parameters of the region.

An increasing number of theoretical and semi-empirical approaches try to explain the stellar mass spectrum, e.g., Silk (1977), Padoan et al. (1997), Murray & Lin (1996), Elmegreen (1998), Adams & Fatuzzo (1996), Bonnell et al. (1997), Myers (2000), and recent models discussed at this conference. Despite numerous and diverse approaches none of the concepts seems to be capable of predicting the stellar mass spectrum under the extreme conditions in starbursts. Hence, observational input is needed!

[1] W. Brandner, F. Eisenhauer, A.F.J. Moffat, F. Palla & H. Zinnecker

[2] H. Zinnecker, W. Brandner, A. Moneti, D. Hunter, M. McCaughrean, G. Meylan, R. Larson, M. Rosa, N. Walborn & G. Weigelt

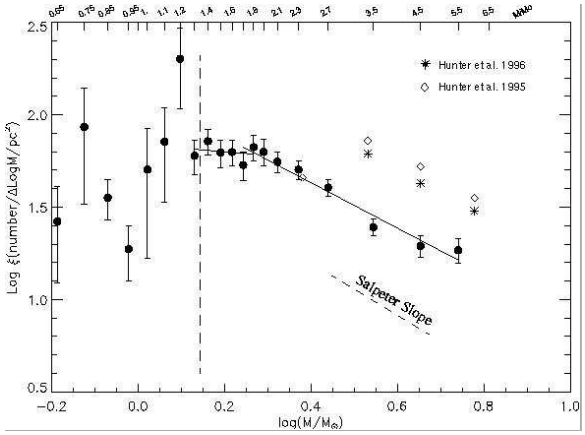

Figure 1. A "definite flattening below $\sim 2M_\odot$" of the IMF in 30 Doradus was found by Sirianni et al. (2000), based on very deep V and I broadband WFPC2 images from the HST archive.

Evidence for a different IMF in star-forming regions has been found in several observational studies: the element abundances in spiral arms/interarm regions ($m_l \geq 2M_\odot$ [Güsten & Mezger 1982]), the metal abundances in galaxy clusters ($\rightarrow$ top-heavy IMF), cooling flows in galaxy clusters ($\rightarrow$ bottom-heavy IMF), and studies of isolated LMC/SMC associations ($\Gamma \approx 3.5$ [Massey et al. 1995]). Maybe the strongest support for a substantially higher low-mass cut-off in starbursts came from a comparison of radiation *and* gravitation for M82, suggesting $m_l \sim 3 - 5M_\odot$ (Rieke et al. 1993). However, starburst modelling is a tricky business and depends on various assumptions, and a similar analysis of M82 by Satyapal et al. (1995) did not confirm the high value of m_l.

Recently, Sirianni et al. (2000) have investigated the low-mass end of the IMF around R136 based on very deep WFPC2 images in V and I band from the HST archive and extended the mass range below Hunter et al.'s (1995) limit of $2.8M_\odot$. The authors find that "after correcting for incompleteness, the IMF shows a definite flattening below $\sim 2M_\odot$" (Fig. 1). However, their conclusion is based only on regions $r \geq 1.5\,\mathrm{pc}$ *around* R136 and it remains unclear whether the conditions there are still representative of dense starburst cores. On the other hand, most stars less massive than $\sim 2 - 3M_\odot$ show varying amounts of extinction due to circumstellar disks or envelopes, which — if the observations are performed at optical wavelengths — require a magnitude-limit correction (Selman et al. 1999) in addition to correction for incompleteness.

Most observational methods used to study starburst regions are based on nebular emission lines, far-IR fluxes, UV stellar winds, and red supergiant spectral features — diagnostics which are most sensitive to OB stars with little information on the low-mass star content. The best way to get an accurate census of the entire stellar population is through the detection of individual stars by means of high angular resolution techniques at near-IR wavelength. The near-IR is the ideal wavelength range for these studies since extinction is significantly reduced ($A_K \sim 0.11A_V$, Rieke & Lebofsky [1985]) and the difference in luminosity between young stars spanning three orders of magnitude in mass is

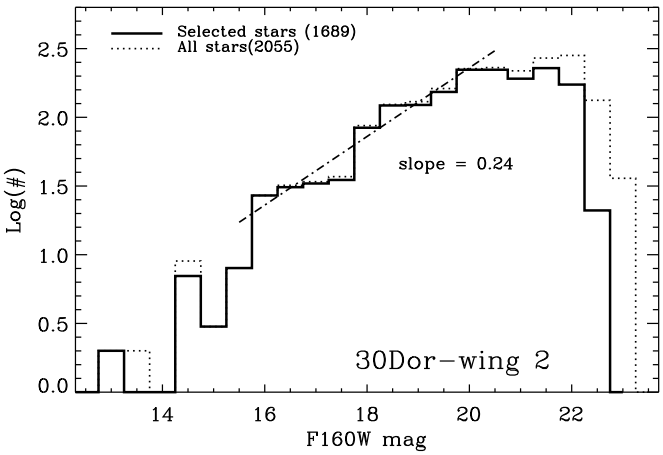

Figure 2. Infrared luminosity function (F160W, NIC2) for "wing 2" in 30 Dor. 'Selected stars' refers to stars with a magnitude error $\leq$ 0.2 mag were considered (solid line) [Zinnecker et al. 1998].

reduced by a large factor compared to optical wavelengths, while still providing sufficient theoretical angular resolution on large telescopes.

The range of regions with intense star formation stretches from ultra-luminous galaxies to massive H II regions. Unfortunately, only the closest regions provide the possibility to identify stars in the sub-solar mass range. However, recent studies of starburst galaxies using the Short-Wavelength Spectrometer (SWS) onboard ESA's Infrared Space Observatory ISO (Thornley et al. 2000) and complementary ground-based near-IR spectroscopy (Förster-Schreiber 1998) indicate that starburst activity occurs on parsec scales in regions of various sizes and locations which have very similar properties. We conclude that 30 Doradus and NGC 3603 are representative building blocks of more distant and luminous starbursts, and use them to address the following questions:

- Is the stellar population produced in starbursts significantly different from the stars born in less violent evironments?
- Do low- and high-mass stars form simultaneously?
- What is the spatial distribution of low- and high-mass stars?
- Do low-mass stars form at all?

2. R 136

With $8\times10^5 M_\odot$ of gas, ionized by 10^{52} Lyman-continuum photons/s (Kennicutt 1984), and a surface brightness of $8\times10^7 L_\odot$ at its core R136, 30 Doradus is the most luminous starburst region in the Local Group. At a distance of 53 kpc it is possible to spatially resolve most of the stellar content of its ionizing cluster NGC2070, which contains about 2400 OB stars (Parker 1993).

We observed the 30 Doradus region with NICMOS onboard HST during 26 orbits to establish the H-band luminosity function down to the faintest practical

Figure 3. F160W ("H-band") HST/NIC1 image of R136 in logarithmic scaling. Pixel scale is $0\farcs043$/pixel for best spatial sampling, the FOV is $11'' \times 11''$ ($2.8 \times 2.8\,\mathrm{pc}^2$).

limit. Most observations were carried out with the NIC2 camera which provides a $0\farcs075$/pixel scale ($20''\times20''$ field of view, FOV). Although slightly undersampled, we've chosen this mode because of its superior sensitivity and large field of view. The observations consist of a 3×3 ($56'' \times 56''$) mosaic centered on R136, and two 3×1 ($56'' \times 20''$) wings extending away from the core. All observations were obtained in MULTIACCUM mode (see Zinnecker & Moneti (1998) for details) and four dithered images were obtained for each position to remove bad pixels, cosmic rays, and the coronographic hole. Photometry was measured with DAOphot (Stetson 1987). No color correction or conversion from F160W to a "standard" H-magnitude has been made; however, comparisons with ground-based magnitudes for individual stars in R136 (Brandl et al. 1996) indicate photometric uncertainties of ≤ 0.2 mag (Zinnecker et al. 1998).

The main goal of these observations was to establish the first deep infrared luminosity function of the 30 Doradus region — our "wing 2" is located Northwest at $r > 15''$ from R136 where crowding is less severe. We have detected *for the first time* pre-main sequence stars below $1M_\odot$ ($H \approx 21^\mathrm{m}$). The luminosity function shows an apparent turnover — probably due to incompleteness — at around $H \approx 20^\mathrm{m}$ (Fig. 2). For the range from $H = 16^\mathrm{m}$ to $H = 20^\mathrm{m}$ where our sample is almost complete we determined the IMF slope Γ using the time-dependent pre-MS mass-luminosity-relation $L_H \sim M^{-1.4}$ for an assumed cluster age of 2 Myr, based on d'Antona & Mazzitelli (1994) tracks and dwarf colors.

We find $\Gamma = 0.84$, which is flatter than the Salpeter IMF slope of $\Gamma = 1.35$, but very similar to $\Gamma = 0.79$ found in NGC 3603 by Eisenhauer et al. (1998).

Most importantly perhaps, our results do not confirm the finding by Sirianni et al. (2000) mentioned above, i.e., we find no clear evidence for a significant turnover above $1M_{\odot}$.

In addition to the NIC2 data we've also obtained NIC1 ($0\farcs043$/pixel) images for better spatial sampling on the central $11'' \times 11''$ ($2.8 \times 2.8\,\mathrm{pc}^2$) around R136. The resulting image is composed of four exposures of 960s each and shown in Fig. 3. Due to the significant crowding and extended diffraction structure in the NICMOS PSF we've chosen a different analysis approach: In the first step we analyzed the images with DAOfind (Stetson 1987) to detect the positions of the brightest sources. Next we used PLUCY (Hook et al. 1994) to derive the photometric fluxes for these sources and produce a map from which the detected sources have been removed. PLUCY accounts for the full structure of the PSFs within the FOV – this is important in our case where very faint objects are close to the diffraction spikes of a bright point source. The PLUCY output map was used for subsequent source position detections using DAOfind. The resulting source list and the original source list were combined and PLUCY was run again. These steps were repeated iteratively 4 times. In total we found about 1850 sources in the field.

Despite this sophisticated approach the non-detection of an existing source due to crowding is the limiting factor in this analysis. We determined the level of incompleteness by randomly adding artificial stars with a flux distribution following the Salpeter IMF and density following approximately the cluster profile to the original image and reanalyzing it through the same procedures as the original image. To avoid introducing systematic errors by adding a large number of stars at once we added only 350 stars at one time and repeated the analysis two times, which makes it a time consuming procedure. We determined the detection probability as a function of apparent magnitude and distance from the cluster center and applied this correction factor to the number of stars detected in each luminosity bin. The result is shown in Fig. 4.

After correction for incompleteness, the H-band luminosity function at $r > 1\,\mathrm{pc}$ ($4''$) around the cluster center but within our $11'' \times 11''$ FOV shows no clear evidence for a truncation down to about $1M_{\odot}$, which is in excellent agreement with our above NIC2 results on the surroundings. Below $1M_{\odot}$ where the uncertainties from completeness correction become significant no statement can be made.

Inside the central parsec ($4''$) we detect about a thousand sources. The luminosity function in the core is flatter compared to the outer parts of the cluster. For $H \geq 19^{\mathrm{m}}$ less than 10% of the sources — whether they exist there or not — can be detected, and incompleteness due to crowding does *not* permit us to reach below $2.5M_{\odot}$. The only way to go significantly deeper in the center is to either wait for NGST and high-order adaptive optics on 8m class telescopes, or to study targets which are very similar to but closer than R136. For now we will follow the latter way.

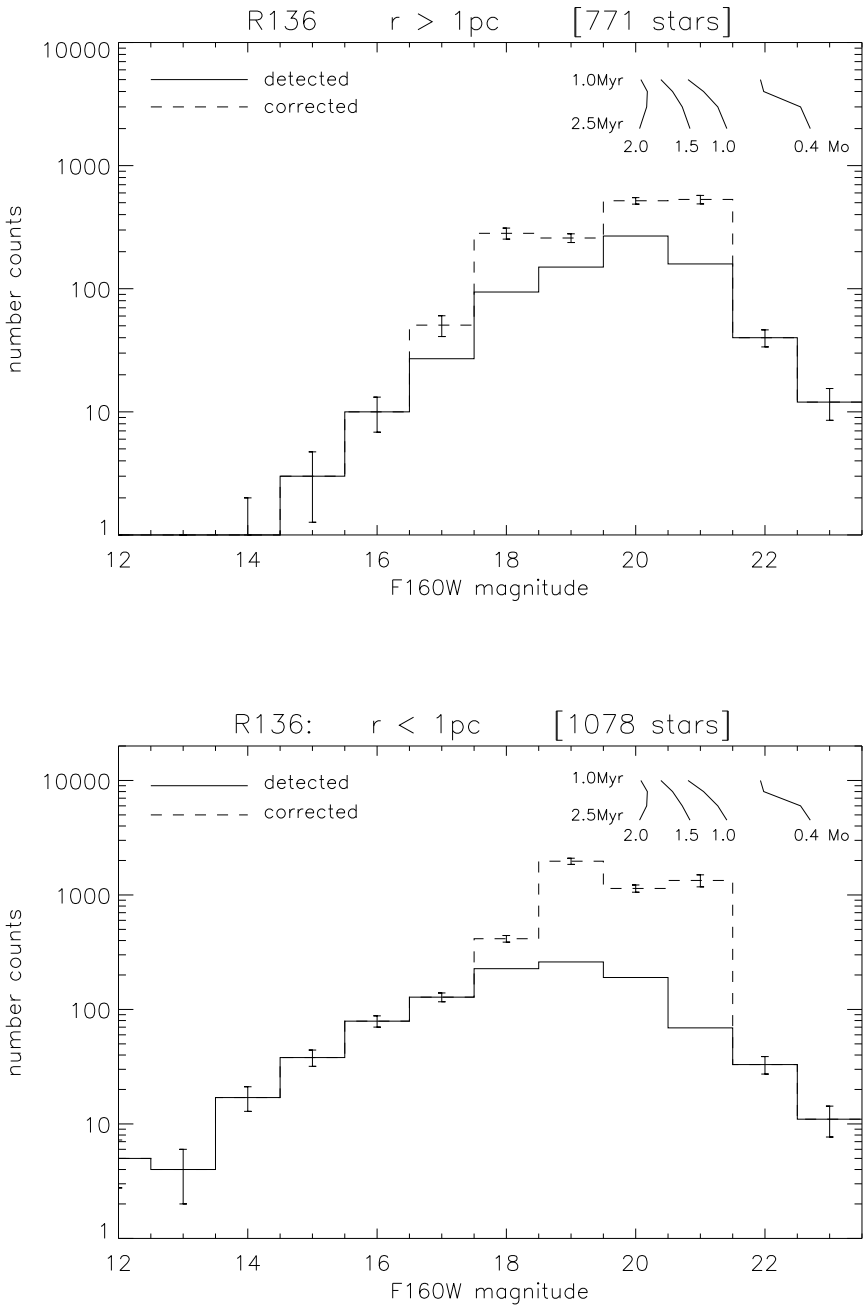

Figure 4. F160W luminosity function for about 1850 stars with $r > 1\,\mathrm{pc}$ (top) and $r < 1\,\mathrm{pc}$ (bottom) within the NIC1 $11'' \times 11''$ FOV. The dotted line represents the number of actually detected stars whereas the dashed line is corrected for incompleteness. The error bars are purely statistical based on the number of detected stars. The upper right part of both diagrams indicates the according pre-MS stellar masses of $0.4, 1.0, 1.5, 2.0 M_{\odot}$ for ages reaching from 1 to 2.5 Myr (Palla & Stahler 1999).

Figure 5. Grey-scale version of a J_s, H, and K_s composite of NGC 3603. Intensities are scaled in logarithmic units; FOV is $3\farcm4 \times 3\farcm4$ (6.2×6.2 parsec^2). North is up, East to the left. The insert to the lower right is a blow up of the central parsec^2. For a color version see Brandl et al. (1999). The image also shows the three proplyd-like objects that have been recently discovered by Brandner et al. (2000); these "proplyds" are similar to those seen in Orion but about 20-30 times more extended. About $1'$ south of the central cluster, we detect the brightest members of the deeply embedded proto-cluster IRS 9.

3. NGC 3603

The densest concentration of massive stars in the Milky Way — and the only massive, Galactic H II region whose ionizing central cluster can be studied at optical wavelengths due to only moderate (mainly foreground) extinction of $A_V \approx 4.5^m$ (Eisenhauer et al. 1998) — is NGC 3603 (HD97950). At a distance of only 6 kpc (De Pree et al. 1999) NGC 3603 is very similar to R136 (Moffat, Drissen & Shara 1994). With a bolometric luminosity of $10^7 L_\odot$ and more than 50 O and WR stars but only $\frac{1}{50}$ of the ionized gas mass of 30 Doradus, NGC 3603 is even denser in its core than R136. With a Lyman continuum flux of $10^{51} s^{-1}$ (Kennicutt 1984; Drissen et al. 1995) NGC 3603 has about 100 times the ionizing power of the Trapezium cluster in Orion.

We observed NGC 3603 in the $J_s = 1.16 - 1.32\mu$m, $H = 1.50 - 1.80\mu$m, and $K_s = 2.03 - 2.30\mu$m broadband filters using the near-IR camera ISAAC mounted on ANTU, ESO's first VLT. The service mode observations were made

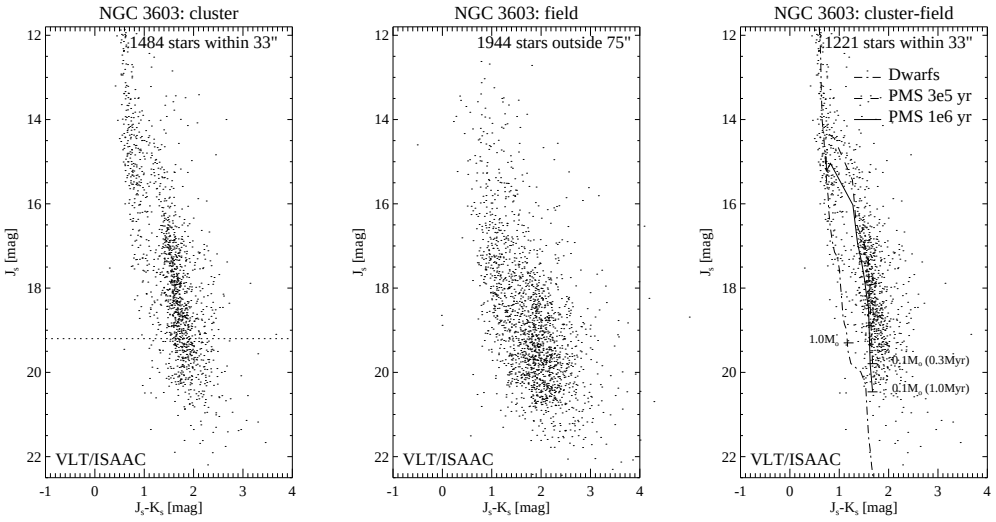

Figure 6. **a-c.** $J_{\rm s}$ versus $J_{\rm s} - K_{\rm s}$ color-magnitude diagrams of NGC 3603. **a** contains all stars detected in all three wavebands within the central $r \leq 33''$ (1 pc) [$1'^2$], **b** shows the field stars at $r \geq 75''$ (2.25 pc) [$6.3'^2$] around the cluster, and **c** shows the cluster population within $r \leq 33''$ with the field stars statistically subtracted. The dashed horizontal line in **a** indicates the detection limit of the previous most sensitive NIR study by Eisenhauer et al. (1998). **c** also shows the theoretical isochrones of pre-main sequence stars of different ages from Palla & Stahler (1999) and the main sequence for dwarfs. For comparison we've plotted some corresponding stellar masses next to the isochrones.

in April 1999 when the optical seeing was equal or better than $0.''4$ on Paranal. Such seeing was essential for accurate photometry in the crowded cluster and increased our sensitivity to the faintest stars. The details of the data reduction and calibration are described in Brandl et al. (1999). The effective exposure times of the final broadband images in the central $2.'5 \times 2.'5$ are 37, 45, and 48 minutes in $J_{\rm s}$, H, and $K_{\rm s}$, respectively. The images resulting from dithering are $3.'4 \times 3.'4$ in size with pixels of $0.''074$ (Fig. 5).

In order to derive photometric fluxes of the stars we used the IRAF implementation of DAOphot (Stetson 1987). We first ran DAOfind to detect the individual sources, leading to ∼20,000 peaks in each waveband. Many of these may be noise or peaks in the nebular background and appear only in one waveband. In order to reject spurious sources, which may be misinterpreted as a low-mass stellar population, we required that sources be detected independently in all three wavebands, and that the maximal deviation of the source centroid between different wavebands be less than $0.''075$. The resulting source list contains about 7000 objects in the entire FOV, which were flux calibrated using faint NIR standard stars from the lists by Hunt et al. (1998) and Persson et al. (1998) [see Brandl et al. (1999) for details].

Fig. 6**a** shows the color-magnitude diagram (CMD) for all stars detected in all 3 wavebands within $r \leq 33''$ (1 pc). Since NGC 3603 is located in the Galactic Plane and 9 times closer than R136 we expect a significant contamination from field stars. To reduce this contribution we followed a statistical approach by subtracting the average number of field stars found in the regions around the cluster at $r \geq 75''$ (Fig. 6**b**) per magnitude and per color bin (0.5 mag each). The accuracy of our statistical subtraction is mainly limited by three factors: first, low-mass pre-main sequence stars are also present in the outskirts of the cluster; second, the completeness limit varies across the FOV; third, local nebulosities may hide background field stars. However, none of these potential errors affects our conclusions drawn from the CMD.

The resulting net CMD for cluster stars within $r \leq 33''$ of NGC 3603 is shown in Fig. 6**c**. We overlayed the theoretical isochrones of pre-main sequence stars from Palla & Stahler (1999) down to $0.1 M_{\odot}$. We assumed a distance modulus of $(m-M)_{\rm o} = 13.9$ based on the distance of 6 kpc (De Pree et al. 1999) and an average foreground extinction of $A_{\rm V} = 4.5^{\rm m}$ following the reddening law by Rieke & Lebofski (1985).

The upper part of the cluster-minus-field CMD clearly shows a main sequence with a marked knee indicating the transition to pre-main sequence stars. The turn-on occurs at $J_{\rm s} \approx 15.5^{\rm m}$ ($m \approx 2.9 M_{\odot}$). Below the turn-on the main-sequence basically disappears. We note that the width of the pre-main sequence in the right part of Fig. 6**c** does not significantly broaden toward fainter magnitudes, indicating that our photometry is not limited by photometric errors. In fact, the scatter may be real and due to varying foreground extinction, infrared excess and different evolutionary stages. In that case the left rim of the distribution would be representative of the "true" color of the most evolved stars while the horizontal scatter would be primarily caused by accretion disks of different inclinations and ages. Fitting isochrones to the left rim in the CMD yields an age of only $0.3 - 1.0$ Myr. Our result is in good agreement with the study by Eisenhauer et al. (1998) but extends the investigated mass range by about one order of magnitude toward smaller masses.

Fig. 7 shows the $J_{\rm s}$ and $K_{\rm s}$ luminosity functions for stars detected in all 3 wavebands with no correction for incompleteness applied, i.e, toward fainter magnitudes an increasing number of stars will remain undetected. Thus we cannot say whether the apparent turnover at $K_{\rm s} \approx 16.5^{\rm m}$ is real or an observational artifact, but we can state that the mass spectrum is well populated down to at least $0.1 M_{\odot}$ assuming an age of 0.7 Myr for a pre-MS star with $K_{\rm s} \sim 19^{\rm m}$.

4. Conclusions

We have studied the stellar content of the two closest, most massive starburst regions NGC 3603 and 30 Doradus. Our studies using HST/NICMOS and VLT/ISAAC are the most sensitive made to date of dense starburst cores. The NIR luminosity function of 30 Doradus shows *no* evidence for a truncation down to at least $1 M_{\odot}$, its stellar core R136 is populated in low-mass stars to at least $2 M_{\odot}$ and NGC 3603, which is very similar to R136, down to $0.1 M_{\odot}$. In a more general picture our findings on starburst cores are:

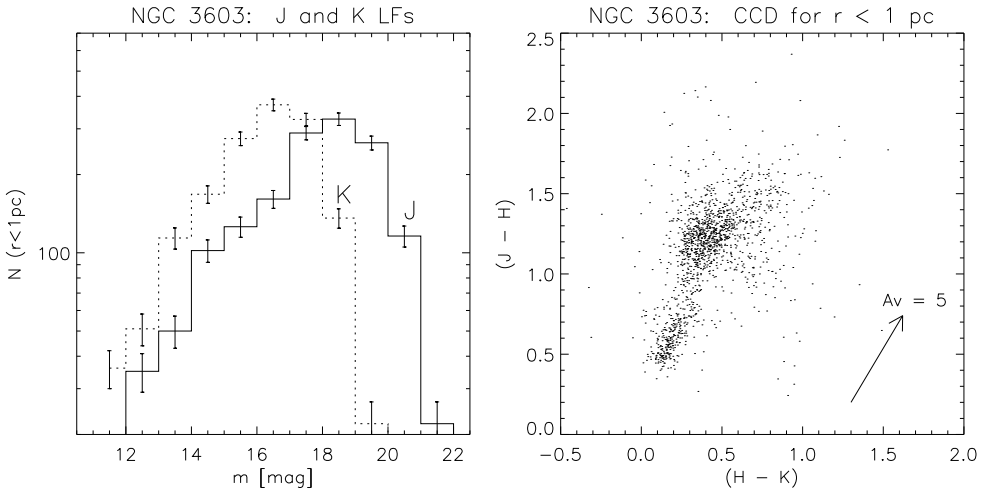

Figure 7. Left: J_s (solid) and K_s-band (dashed) luminosity functions of stars detected at all 3 wavebands in the central stellar cluster within $r \leq 33''$ (1 pc). The number counts have not been corrected for incompletenes; error bars are purely statistical. Right: Color-color diagram for the same 1500 stars within 1 pc of the center. Redder and younger stars are located toward the upper right.

- There is no clear evidence for an anomalous IMF.
- The slope of the IMF tends to flattens toward the center.
- There is no evidence for a low-mass cutoff above our completeness limits.
- Sub-solar mass stars do form in large numbers in violent star forming regions and are present throughout the cluster.

Acknowledgments. B.B. wants to thank the organizers, in particular Thierry Montmerle and Philippe André, for a very stimulating meeting in a beautiful setting.

References

Adams, F.C. & Fatuzzo, M. 1996, ApJ, 464, 256

Bonnell, I.A.; Bate, M.R., Clarke, C.J., Pringle, J.E. 1997, MNRAS, 285, 201

Brandl, B., Sams, B.J., Bertoldi, F., Eckart, A., Genzel, R., Drapatz, S., Hofmann, R., Loewe, M., Quirrenbach, A. 1996, ApJ, 466, 254

Brandl, B., Brandner, W. & Zinnecker, H. 1999, Star Formation 1999, eds. T. Nakamoto et al., in press'

Brandner, W., Grebel, E.K., Chu, Y-H., Dottori, H., Brandl, B., Richling, S., Yorke, H.W., Points, S.D., Zinnecker, H. 2000, AJ, 119, 292

d'Antona, F. & Mazzitelli, I. 1994, ApJS, 90, 467

De Pree, C.G., Nysewander, M.C. & Goss, W.M. 1999, AJ, 117, 2902

Drissen, L., Moffat, A.F.J., Walborn, N. & Shara, M.M. 1995, AJ, 110, 2235

Eisenhauer, F., Quirrenbach, A., Zinnecker, H. & Genzel, R. 1998, ApJ, 498, 278

Elmegreen, B. 1998, ApJ, 486, 944

Förster-Schreiber, N.M. 1998, PhD thesis, Ludwig-Maximilians-University Munich

Güsten, R. & Mezger, P.G. 1982, Vistas Astr., 26, 159

Hook, R. et al. 1994, ST-ECF Newsletter, 21, 17

Hunt, L.K., Mannucci, F., Testi, L., Migliorini, S., Stanga, R.M., Baffa, C., Lisi, F., Vanzi, L. 1998, AJ, 115, 2594

Hunter, D.A., Shaya, E.J., Holtzman, J.A., Light, R.M., O'Neil, E.J.Jr., Lynds, R. 1995, ApJ, 448, 179

Kennicutt, R.C.Jr. 1984, ApJ, 287, 116

Kroupa, P., Tout, C.A. & Gilmore, G. 1990, MNRAS, 244, 76

Massey, P., Lang, C.C., Degioia-Eastwood, K., Garmany, C.D. 1995, ApJ, 438, 188

Miller, G.E. & Scalo, J.M. 1979, ApJS, 41, 513

Moffat, A.F.J., Drissen, L., & Shara, M.M. 1994, ApJ, 436, 183

Murray, S.D. & Lin, D.N.C. 1996, ApJ, 467, 728

Myers, P.C. 2000, ApJ, L530, 119

Padoan, P. et al. 1997, MNRAS, 288, 145

Palla, F. & Stahler, S.W. 1999, ApJ, 525, 772

Parker, J.W. 1993, AJ, 106, 560

Persson, S.E., Murphy, D.C., Krzeminski, W., Roth, M., Rieke, M.J. 1998, AJ, 116, 247

Rieke, G.H. & Lebofsky, M.J. 1985, ApJ, 288, 618

Rieke, G.H., Loken, K., Rieke, M.J., Tamblyn, P. 1993, ApJ, 412, 99

Salpeter, E.E. 1955, ApJ, 121, 161

Satyapal, S. Watson, D.M., Pipher, J.L., Forrest, W.J., Coppenbarger, D., Raines, S.N., Libonate, S., Piche, F., Greenhouse, M.A., Smith, H.A., Thompson, K.L., Fischer, J., Woodward, C.E., Hodge, T. 1995, ApJ, 448, 611

Scalo, J.M. 1986, Fundam.Cosmic Phys., 11, 1

Selman, F., Melnick, J., Bosch, G., Terlevich, R. 1999, A&A, 347, 532

Silk, J. 1977, ApJ, 214, 718

Sirianni, M., Nota, A., Leitherer, C., De Marchi, G., Clampin, M. 2000, ApJ, 533, 203

Stetson, P.B. 1987, PASP, 99, 191

Thornley, M.D., Förster-Schreiber, N.M., Lutz, D., Genzel, R., Spoon, H.W.W., Kunze, D., Sternberg, A. 2000, A&A, in press

Zinnecker, H. & Moneti, A. 1998, ESO Conf. & Workshop Proc. 55, eds. W. Freudling & R. Hook, 136

Zinnecker, H., Brandl, B., Brandner, W., Moneti, A., Hunter, D. 1998, IAU Symp. 190, 24

Zinnecker, H. et al. 2000, in preparation

This figure "figure3.gif" is available in "gif" format from:

http://arXiv.org/ps/astro-ph/0007298v1

This figure "figure5.gif" is available in "gif" format from:

http://arXiv.org/ps/astro-ph/0007298v1